Polyhedron 188 (2020) 114701

Contents lists available at ScienceDirect

Polyhedron

journal homepage: www.elsevier.com/locate/poly

Two new Zn-based coordination polymers constructed from a light responsive organic ligand: Efficient clean-up of Cr(VI) and organic pollutants

Si-Qi Ma [a], Baoyi Yu [b], Xiao-Hong Yi [a], Chong-Chen Wang [a,*]

[a] Beijing Key Laboratory of Functional Materials for Building Structure and Environment Remediation, Beijing University of Civil Engineering and Architecture, Beijing 100044, China
[b] Key Laboratory of Urban Agriculture (North China), Ministry of Agriculture, College of Biological Sciences Engineering, Beijing University of Agriculture, Beijing 102206, China

ARTICLE INFO

Article history:
Received 12 March 2020
Accepted 2 July 2020
Available online 11 July 2020

Keywords:
Coordination polymer
Photocatalysis
Cr(VI) reduction
Organic dyes
Clean-up

ABSTRACT

Two new coordination polymers, ZnL(2,2′-bpy)·(H_2O) (**BUC-85**) and ZnL(bpa)·(H_2O) (**BUC-86**) (H_2L = *cis*-1,3-dibenzyl-2-imidazolidone-4,5-dicarboxylic acid, 2,2′-bpy = 2,2′-bipyridine, bpa = 1,2-bis(4-pyridyl) ethane), were synthesized under solvothermal conditions. The abilities of both **BUC-85** and **BUC-86** were tested for photocatalytic Cr(VI) reduction and organic pollutant degradation under UV light. The results revealed that both **BUC-85** and **BUC-86** displayed superior catalytic Cr(VI) reduction performances, with reduction efficiencies up to 99% within 40 min under UV light irradiation. As well, **BUC-85** and **BUC-86** could photocatalytically decompose organic dyes, in which the oxidative degradation efficiencies toward methylene blue were 100% (**BUC-85**) and 99% (**BUC-86**) under irradiation of UV light for 60 min. Finally, a possible photocatalytic reaction mechanism has been proposed and verified.

1. Introduction

Nowadays, water resources and water quality have attracted worldwide attention. However, heavy metals and organic pollutants in water are difficult to remove, and they can exerted great harm to human, aquatic animals and plants [1–4]. The Cr(VI) ion, as one of the most common types of heavy metal ion, mainly comes from electroplating production, stainless steel products, leather and other industries [5–8]. The presence of Cr(VI) ions in the water environment will increase the risk to human health with regard to liver, kidney, skin and mucosa problems [9]. As the Cr(III) ion is less toxic to the human body and can be easily removed as Cr$(OH)_3$ precipitates, the strategy of transforming Cr(VI) ions into Cr(III) ions is often adopted [10–12].

Generally, heavy metals (like Cr(VI) ions) and organic pollutants (like organic dyes) coexist in wastewater [13,14]. Up until now, conventional methods like adsorption, chemical precipitation, biological treatment, membrane filtration are often used to remove Cr(VI) ions from wastewater [15–17], which are limited due to disadvantages like mass sludge production, high chemical consumption, high processing cost and poor sustainable development. The photocatalytic method not only can reduce Cr(VI) ions into Cr(III) ions, but also degrade organic dyes into biologically degradable intermediates or even CO_2 [18,19]. Thus, the discovery of effective photocatalysts is a key challenge to be considered.

Coordination polymers (CPs) are composed of metal atoms as templates and organic ligands with different functional groups as linkers [20,21], which has attracted increasing concerns in varied research fields, including but not limited to gas adsorption/separation [22], adsorptive removal of pollutants [23], luminescent sensing [20,24] and bacteriostatic agents [25]. Especially, some CPs have been widely used as photocatalysts to achieve CO_2 reduction [26,27], H_2 production [28,29] and pollutant elimination [30].

Our group firstly adopted *cis*-1,3-dibenzyl-2-imidazolidone-4,5-dicarboxylic acid (H_2L) ligand to synthesize a series of effective UV light responsive photocatalysts, like **BUC-18** (Cd(bpp)(H_2O)L) [31], **BUC-19** (Zn(bpp)L) [31], **BUC-20** ($[Cu^{II}(L)_2][Cu^{I}(bpy)]_2{\cdot}4H_2O$) [5], **BUC-21** (Zn(bpy)L) [32], **BUC-66** ($[Cd(bpy)(H_2O)L]_n$) [33] and **BUC-67** ($\{Co(bpy)(H_2O)L{\cdot}H_2O\}_{2n}$) [33], to obtain outstanding photocatalytic performances toward Cr(VI) ion and organic dye elimination. To provide novel CPs with different structures, in this work **BUC-85** and **BUC-86** have been synthesized from the hydrothermal reaction between H_2L, 2,2′-bpy/bpa and $Zn(CH_3COO)_2$ salts. Their photocatalytic abilities toward pollutant elimination and the possible corresponding mechanism were clarified.

* Corresponding author.
E-mail address: wangchongchen@bucea.edu.cn (C.-C. Wang).

https://doi.org/10.1016/j.poly.2020.114701
0277-5387/

2. Experimental

2.1. Materials and instruments

The used chemicals and characterization methods are listed in the Supporting Information.

2.2. Synthesis of BUC-85

A mixture of $Zn(CH_3COO)_2$ (0.6 mmol, 131.7 mg), 2,2′-bipyridine (2,2′-bpy, 0.6 mmol, 93.7 mg) and H_2L (0.6 mmol, 212.6 mg) was sealed in a 25 mL Teflon-lined stainless steel Parr bomb including DI water (15 mL), heated at 160 °C for 72 h and then cooled down slowly to room temperature. White block-like crystals of ZnL(2, 2′-bpy)·(H_2O) (**BUC-85**, yield 82% based on $Zn(CH_3COO)_2$) were obtained and washed three times with ethanol and pure water. Anal. Calc. for **BUC-85**, $C_{58}H_{48}N_8O_{10}Zn_2$, C, 60.6; H, 4.2; N, 9.7. Found: C, 60.5; H, 5.1; N, 9.8%. FTIR (KBr) cm^{-1}: 3431, 3060, 3031, 1706, 1654, 1600, 1577, 1495, 1478, 1448, 1424, 1367, 1312, 1253, 1239, 1158, 1076, 1027, 860, 771, 735, 706, 644, 440.

2.3. Synthesis of BUC-86

Pale yellow block-like crystals of ZnL(bpa)·(H_2O) (**BUC-86**, yield 85% based on $Zn(CH_3COO)_2$) were synthesized following the same procedure as for **BUC-85**, except that 2,2′-bipyridine (2,2′-bpy) was replaced by 1,2-bis(4-pyridyl)ethane (bpa). Anal. Calc. for **BUC-86**, $C_{31}H_{28}N_4O_5Zn$, C, 60.0; H, 4.8; N, 9.0. Found: C, 59.8; H, 6.3; N, 8.8%. FTIR (KBr) cm^{-1}: 3388, 3062, 2933, 1692, 1637, 1560, 1496, 1449, 1435, 1304, 1268, 1232, 1189, 1072, 1030, 832, 818, 761, 733, 703, 645, 607, 556, 526, 489.

3. Results and discussion

3.1. Characterization

In the FTIR spectra of **BUC-85** and **BUC-86** (Fig. S1), the intense absorption of the two coordination polymers at 3431 and 3488 cm^{-1} can be ascribed to O—H bonds from lattice water and absorbed water molecules [34]. The peaks at 1637 (**BUC-86**) and 1654 cm^{-1} (**BUC-85**) affirm the existence of υ(—C—O—) vibrations of the L ligands. The wide bands at 526–733 (**BUC-86**) and 644–735 cm^{-1} (**BUC-85**) originate from υ(—Zn—O—) vibrations and confirm the formation of a Zn-O coordination bond [35]. Finally, the coordinative interaction between the Zn^{2+} ions and N atoms from 2,2′-bpy/bpa can be inferred from υ(—Zn—N—) vibrations observed at 489 (**BUC-86**) and 440 cm^{-1} (**BUC-85**) [36].

As shown in Fig. S2, the two CPs displayed similar weight loss processes, though their crystalline structures are disparate. For **BUC-86**, the TGA curve shows three stages of decomposition. The first weight loss of 1.3% (the calculated value being 1.5%) up to 200 °C was assigned to the loss of lattice water molecules. The next loss of 27.2% from 200 to 350 °C was allocated to the removal of the bpa ligand (the theoretical value being 29.6%) and the third weight loss of 49% from 350 to 500 °C resulted from the decomposition of the carboxylate ligand L (the theoretical value being 49.6%). The weight of the final residue, 22.5%, can be attributed to ZnO, in which Zn is 18%, which is in perfect agreement with ZnL(bpa)·(H_2O) (requires 17.9%) [31,37].

3.2. Crystallographic structure analyses

To date, the L ligand has displayed four coordination modes (Scheme 1) in reported coordination polymers like **BUC-18**, **BUC-19**, **BUC-20**, **BUC-21**, **BUC-66**, **BUC-67**, **BUC-85** and **BUC-86**. The two carboxyl groups (—C—O—) in the L ligand are used to coordinate with the central metal atoms (shown in Scheme 1a). Most CPs contain metal ions coordinated by the carboxyl groups (—C═O—), such as **BUC-19**, **BUC-21** and **BUC-86** (shown in Scheme 1b). Three oxygen atoms from one completely deprotonated L^{2-} ligand (—C—O— and —C═O—) are coordinated to metal ion centers (shown in Scheme 1c). Two oxygen atoms and one nitrogen atom from one L ligand are coordinated to metal ion centers (shown in Scheme 1d).

3.2.1. Crystallographic structure analyses of BUC-85

In ZnL(2,2′-bpy)·(H_2O) (**BUC-85**), the Zn(II) ion is five-coordinated in a square pyramidal geometry, by two nitrogen atoms (N3 and N4) from the 2,2′-bpy ligand, two oxygen atoms (O1 and O3) from one completely deprotonated L^{2-} ligand and one oxygen atom (O3A) from another L^{2-} ligand (Fig. 1 and Scheme 1a). The

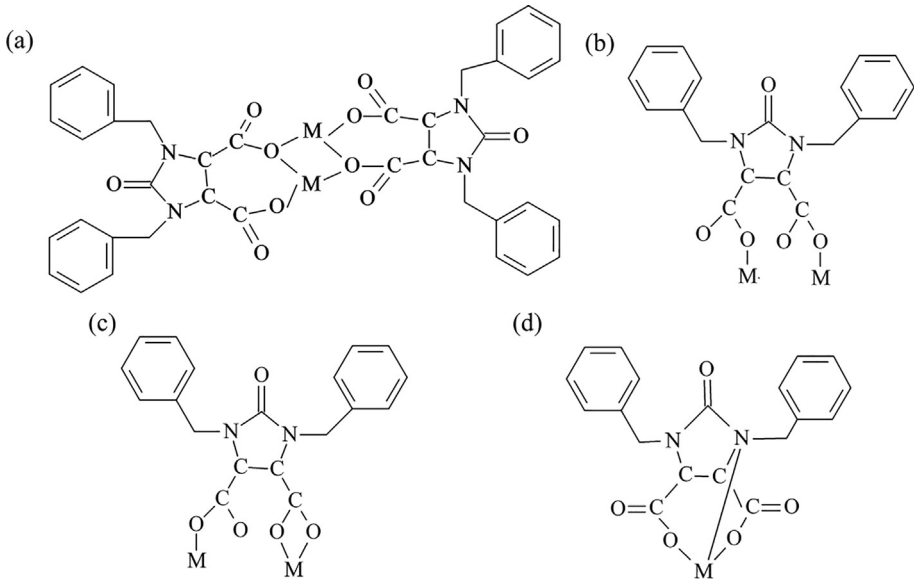

Scheme 1. Coordination patterns of the L ligand in **BUC-85**, **BUC-86, BUC-18** and **BUC-20**.

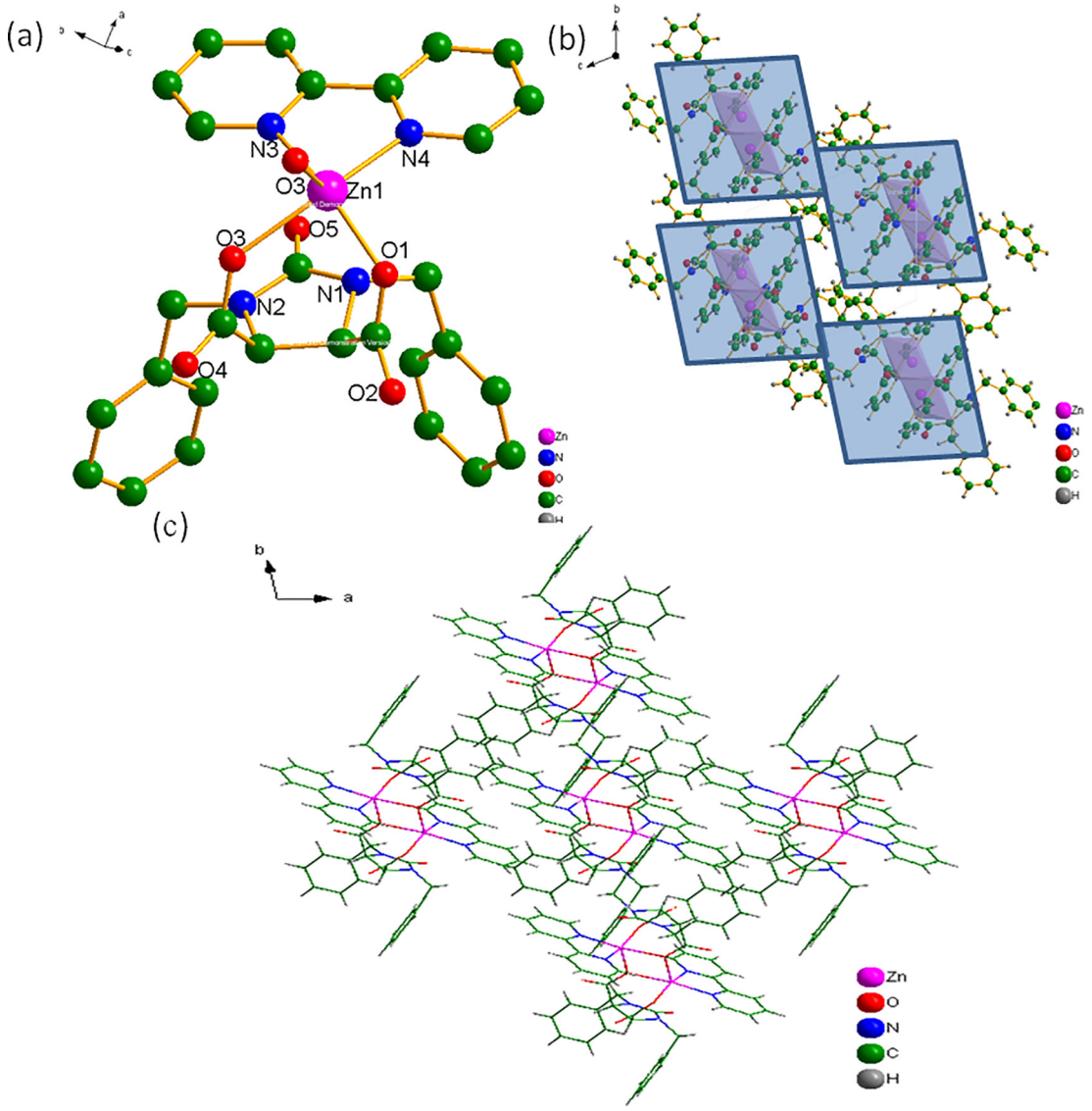

Fig. 1. (a) The asymmetric unit of **BUC-85**; (b) **BUC-85** atomic stacking diagram**.** All the H atoms are omitted for clarity; (c) 3D framework built with the aid of π–π stacking interactions along the c axis.

Zn-O bond distances, ranging from 1.98(19) to 2.05(17) Å, and the Zn-N bond distances, in the range 2.082(2) to 2.089(2) Å, are comparable to typical bonds lengths in the previous reports [38,39] (selected bond lengths and angles are listed in Table S2). In **BUC-85**, the 2,2′-bpy ligand acts as chelating bidentate to coordinate with the Zn^{2+} ion and the L^{2-} ligand exhibits rare tridentate coordination mode [40] to join two different Zn^{2+} templates. Due to the chelating behavior of the 2,2′-bpy ligand, the structure of **BUC-85** is limited as a zero-dimensional unit without further extension. The discrete ZnL(2,2′-bpy)·(H_2O) units are packed into a 3D supramolecular structure with the aid of π-π stacking interactions (Fig. 1c).

3.2.2. Crystallographic structure analyses of BUC-86

In ZnL(bpa)·(H_2O) (**BUC-86**), the Zn(Ⅱ) ion is four-coordinated by two oxygen atoms (O1 and O3) from two completely deprotonated L^{2-} ligands and two nitrogen atoms (N1 and N2) from two bpa ligands, as shown in Fig. 2 and Scheme 1. The Zn-O bond lengths range from 1.946(3) to 1.963(3) Å, and the Zn-N distances range from 2.048(4) to 2.056(4) Å (Table S2), which are in scope for bonds of these types [39,41]. The completely deprotonated L^{2-} ligand, adopting the *trans*-mode, acts as a bis-monodentate ligand to link two Zn(II) ions into an infinite zigzag [ZnL] chain along the *a*-axis (Scheme 1b). As shown in Fig. 2b, adjacent [ZnL] chains are further linked by flexible bpa ligands into a 2D network with an undulating surface, as viewed from the b-axis. Finally, the discrete ZnL(bpa)·(H_2O) units are packed into a 3D supramolecular structure with the aid of π-π stacking interactions.

3.3. Photocatalytic performances

The optical properties of **BUC-85** and **BUC-86** were estimated with a UV–Vis diffuse reflectance spectrophotometer (UV–vis DRS), which revealed that the light absorption bands were at ca. 363 and 375 nm, respectively (Fig. 3). The E_g values were assessed by the Kubelka-Munk function [42], being at ca. 3.6 and 4.1 eV for **BUC-85** and **BUC-86**, indicating that these two CPs can be excited by UV light with a suitable wavelength.

The Cr(VI) reduction efficiencies of free H_2L, P25 (commercial TiO_2), **BUC-85** and **BUC-86** under UV light irradiation are illustrated in Fig. 4(a), in which about 99 and 90% of the Cr(VI) ions were reduced after 20 min with **BUC-85** and **BUC-86** as photocat-

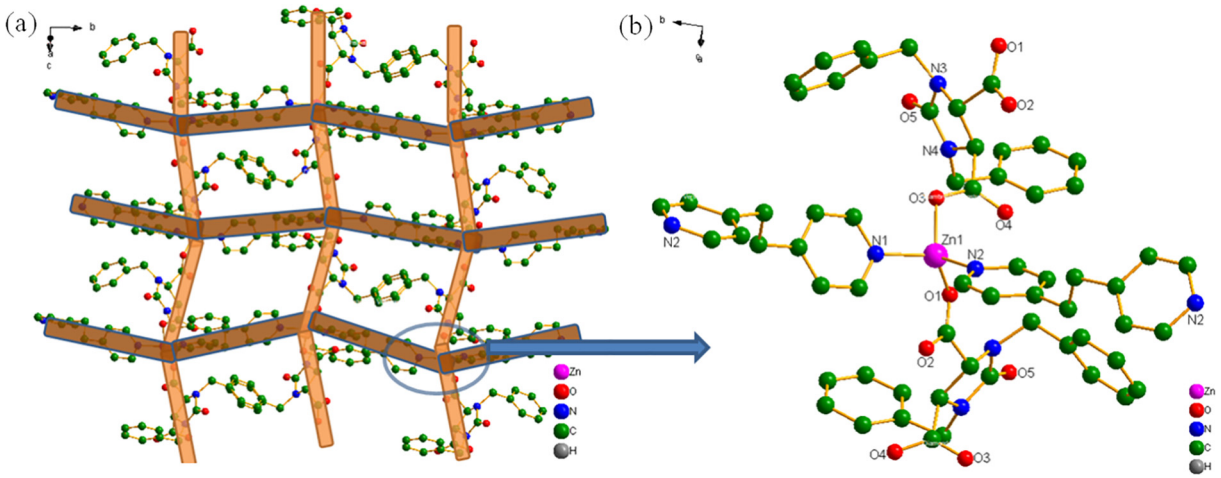

Fig. 2. (a) 2D double layers of **BUC-86** and (b) the asymmetric unit of **BUC-86.** All the H atoms are omitted for clarity.

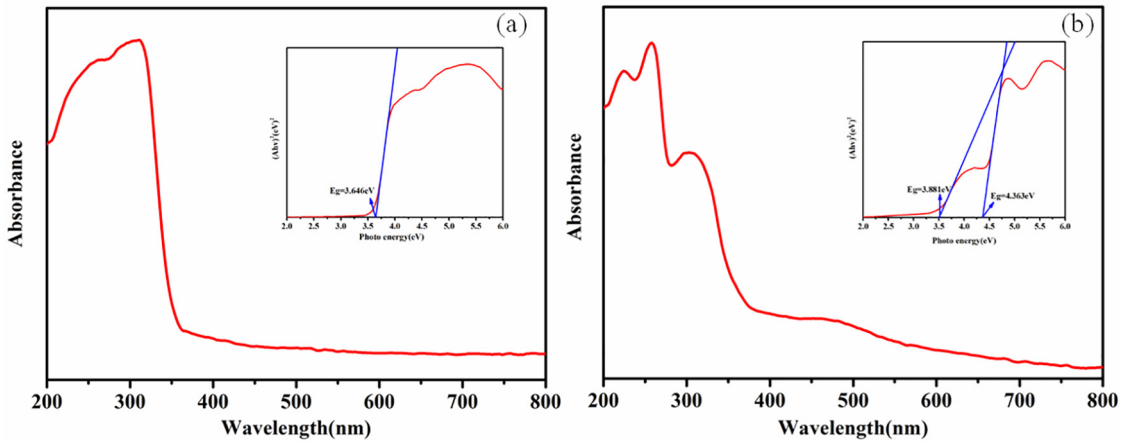

Fig. 3. UV–vis spectra of **BUC-85** (a) and **BUC-86** (b). The inset graph shows the corresponding band gaps of **BUC-85** and **BUC-86**.

alysts, respectively. By comparison, in the presence of free H_2L and P25 as photocatalysts, only 53 and 11% Cr(VI) reduction efficiencies were achieved within 20 min. The removal efficiencies for Cr(VI) ions either without light or without photocatalysts were insignificant [37], signifying that the Cr(VI) reduction could be assigned to the photocatalytic process.

Previous studies reported that the Cr(VI) reduction rate by photocatalysts is greatly influenced by the pH values of the aqueous solution [43]. In Fig. 4b, the Cr(VI) reduction efficiencies over **BUC-85** decreased from 100% at pH 2.0 to 96% at pH 7.0 within 40 min. A similar trend was observed for **BUC-86**, in which the efficiency of Cr(VI) reduction efficiency declined from 100 to 77% within 40 min as the pH increased from 2.0 to 7.0. According to previous reports [44,45], low pH conditions favored the existence of $Cr_2O_7^{2-}$ or $HCrO_4^-$ ions as primary Cr(VI) species and the photocatalytic Cr(VI) reduction followed Eqs. (1) and (2). Higher pH conditions led to the formation of CrO_4^{2-} ions and the Cr(VI) sequestration followed Eq. (3). Some previous reports declared that an alkaline condition would favor the formed Cr(III) ions being transformed into $Cr(OH)_3$ precipitates, which would mask the active sites of the photocatalysts [46]. As for both **BUC-85** and **BUC-86**, their photocatalytic Cr(VI) reduction efficiencies exhibited a slight decline on the increasing pH, however the total Cr(VI) reduction performances were maintained at relatively high levels.

It is well known that the Cr(VI) reduction under neutral condition is expected, as some wastewater containing Cr(VI) ions is neutral or even slightly alkaline [1].

$$\text{BUC-85/86} + h\nu \rightarrow \text{BUC-85/86}\,(e^- + h^+)\ (1)$$

$$Cr_2O_7^{2-} + 14H^+ + 6e^- \rightarrow 2Cr^{3+} + 7H_2O\ (2)$$

$$CrO_4^{2-} + 4H_2O + 3e^- \rightarrow Cr(OH)_3 + 5OH^-\ (3)$$

Three small molecular weight organic acids (oxalic acid, citric acid and tartaric acid) were used to explore the effect of different hole trappings on the Cr(VI) reduction at pH 2.0 (shown in the Fig. S3). Actually, photooxidation of sacrificial organic acids can markedly influence the photoreduction Cr(VI) rate by photo-generated electrons. The consumption of holes (h^+) will accelerate the charge separation of photo-induced electron-hole pairs, resulting in an excellent Cr(VI) reduction efficiency [47,48].

Methylene blue (MB) and methyl orange (MO) were selected to further explore the photocatalytic oxidation performances of **BUC-85** and **BUC-86**. As shown in Fig. 5, the adsorption behaviors of these two selected organic dyes over **BUC-85** and **BUC-86** were negligible. The photocatalytic experiment results revealed 95 and 93% MB is oxidized over **BUC-85** and **BUC-86** as photocatalysts within 40 min under UV light irradiation. These two CPs also

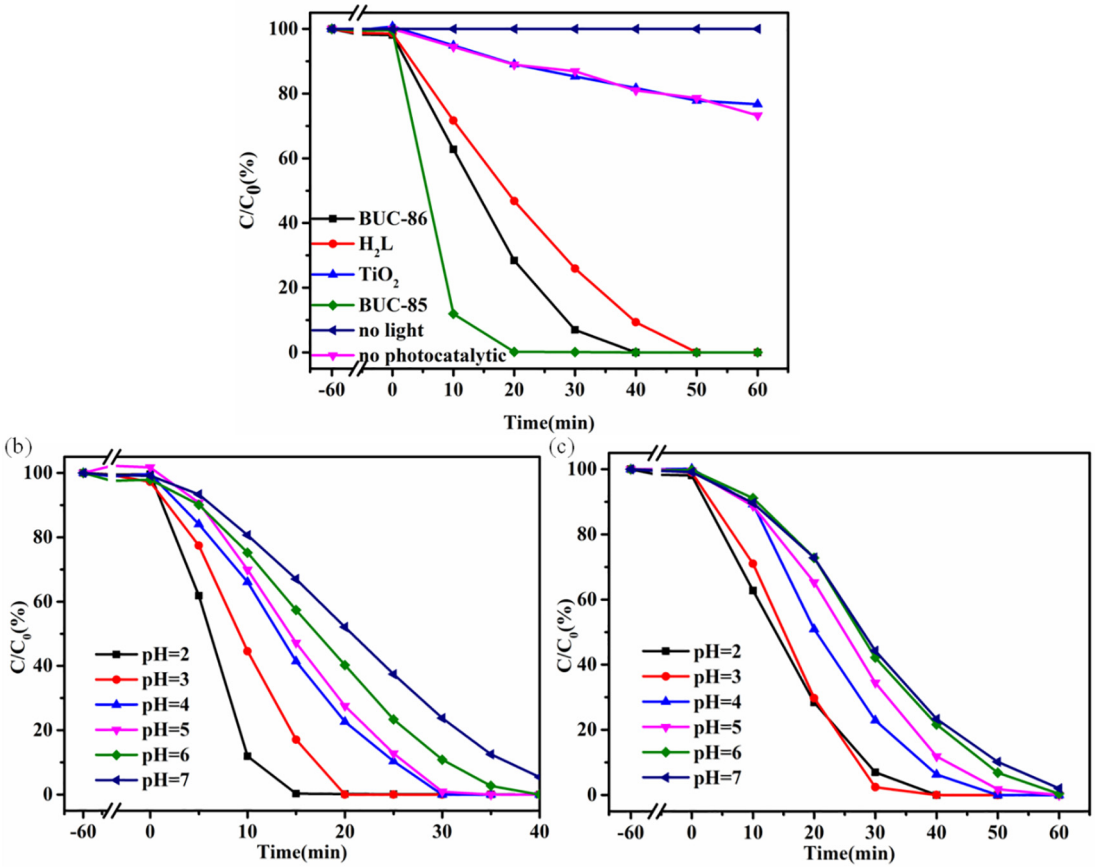

Fig. 4. (a) Cr(VI) photoreduction efficiencies of different photocatalysts. Cr(VI) photoreduction efficiencies of **BUC-85**(b) and **BUC-86**(c) as photocatalysts upon the irradiation of UV light at diverse pH values. Conditions: Cr(VI) = 10 mg/L, volume = 200 mL, pH = 2, photocatalyst dosage = 20 mg.

exhibited outstanding photocatalytic performances toward MO under UV light irradiation, in which **BUC-85** and **BUC-86** can decompose 88 and 63% of MO within 40 min, respectively. In the absence of these two CPs, only ca. 28% MB and 18% MO were removed in up to 40 min, under the UV light irradiation. Using free H_2L as a photocatalyst, ca. 40% MB and 41% MO were decomposed under identical conditions within 40 min. In comparison, 88% MB and 35% MO were destroyed with P25 as a photocatalyst within 40 min. The results indicated that these two new CPs exhibit excellent photocatalytic performances toward both Cr(VI) reduction and organic pollutants degradation.

Several reactive species containing $\cdot O_2^-$ and .OH may participate in photocatalytic reactions for the degradation of organic dyes. Benzoquinone (BQ, 0.2 mmol/L), and isopropanol (IPA, 0.2 mmol/L) were used in photocatalytic trapping experiments as scavengers for $\cdot O_2^-$ and .OH, respectively [49]. In Fig. 6, the MB degradation rate was significantly restrained in the presence of BQ and IPA, indicating that both $\cdot O_2^-$ and .OH were the primary active substances [32].

It is important to evaluate the recyclability and stability of photocatalysts and this was carried out by performing repeated usage cycles under identical reaction conditions. As displayed in Figs. 7 and S4, **BUC-85** and **BUC-86** maintained their excellent photocatalytic activities towards the reduction of Cr(VI) ions for five cycles, along with outstanding MO and MB degradation after three cycles. As for the photocatalytic reduction of Cr(VI) to Cr(III), **BUC-85** demonstrated no obvious decline, however **BUC-86** displayed ca. a 12% decreased on the 5th run. No obvious decrease of the photocatalytic activities toward MB decolorization was observed for **BUC-85** and **BUC-86** during three parallel cycles [50]. It can be seen from Fig. 8 that the PXRD patterns of the used photocatalysts match well with simulated patterns from the single crystal data and the original samples before photocatalysis. The slight differences in intensities may be assigned to the preferred orientations of the crystalline powder samples [51]. In addition, the FTIR and TGA data before and after the photocatalytic reaction displayed no noticeable changes (Figs. S1 and S2), indicating that both **BUC-85** and **BUC-86** are good photocatalyst candidates with outstanding stability.

For the process of practical operation, Cr(VI) ions and organic dyes usually exist at the same time. To further discuss the photoreduction and photodegradation possibilities, the photocatalytic activities of these two CPs for simultaneous Cr(VI) reduction and organic pollutant degradation in Cr(VI)/MB, Cr(VI)/MO and MO/MB mixtures were investigated at pH = 2.0. The removal trends of **BUC-85** (as displayed in Fig. S5) and **BUC-86** (as displayed in Fig. 9) on the mixed system are basically similar, so **BUC-86** is selected to elaborate this further. As shown in Fig. 9a, for the mono-component systems of individual Cr(VI) ions and individual MB solution, **BUC-86** can accomplish 100% Cr(VI) reduction and 94% MB degradation efficiencies within 40 min, respectively. However, the degradation efficiency of Cr(VI) ions and MB were 73 and 37% within 40 min for the Cr(VI)/MB matrix. The rates of Cr(VI) reduction and degradation MB in the matrix were slower than those of the mono-component systems, possibly due to the competition consummation of $\cdot O_2^-$ between Cr(VI) ions and MB. As shown in Fig. 9b, for the mono-component systems of **BUC-86**, the Cr(VI) reduction and MO degradation efficiencies are 100 and 62% within 40 min, respectively. However, the Cr(VI) reduction efficiency was 98% after 40 min in the Cr(VI)/MO matrix, whilst the rate of MO degradation in matrix was faster than for the mono-component

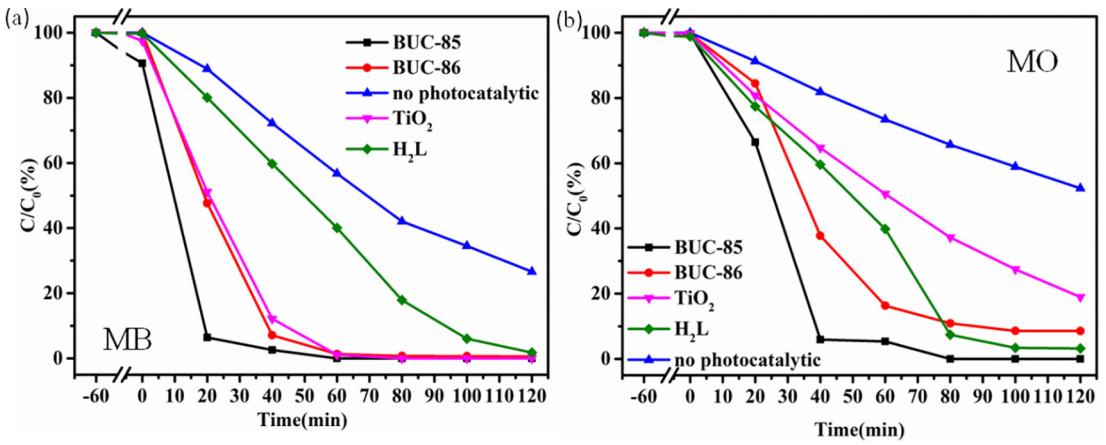

Fig. 5. Photocatalytic oxidation performance of **BUC-85** and **BUC-86** toward (a) MB and (b) MO. Conditions: 200 mL of MO = 10 mg/L or MB = 10 mg/L, photocatalyst dosage = 20 mg.

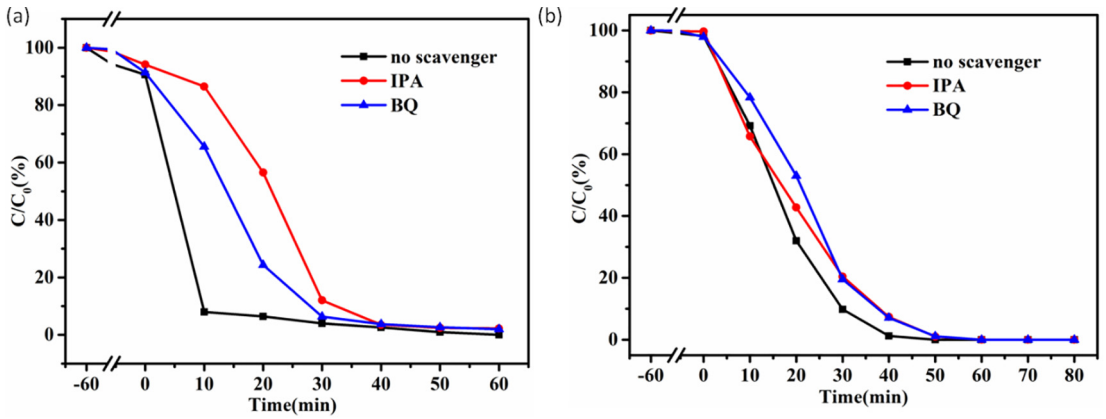

Fig. 6. The outcomes of diverse scavengers on MB oxidation in the presence of **BUC-85** (a) and **BUC-86** (b). Conditions: MB = 10 mg/L, 200 mL, photocatalyst dosage = 20 mg, 0.2 mmol/L scavengers.

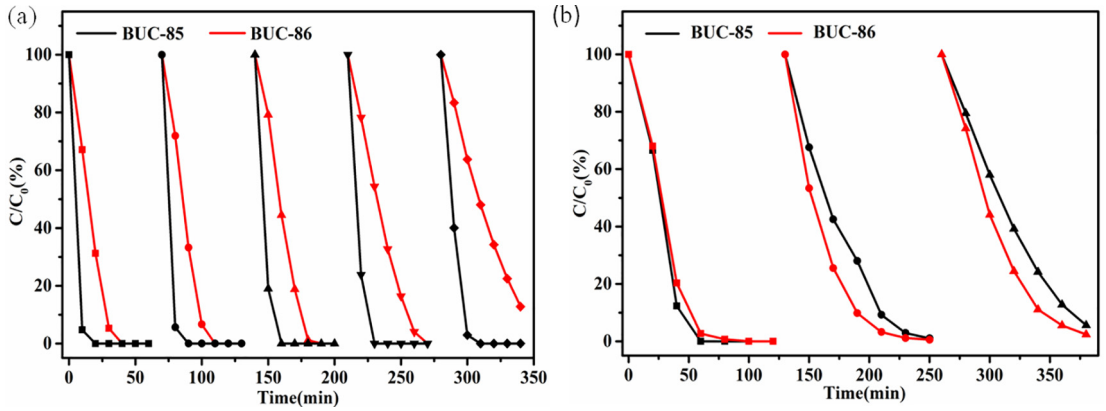

Fig. 7. (a) BUC-85 and **BUC-86** cycling performance for Cr(VI) removal; **(b) BUC-85** and **BUC-86** cycling performance for MB degradation. Conditions: MB = 10 mg/L, 200 mL, photocatalyst dosage = 20 mg, Cr(VI) = 10 mg/L, pH = 2.0.

systems. To explain these observations, it is proposed that the MO was oxidized by not only **.**OH generated from the reaction between H^+ and H_2O, but also by **.**O_2^- radicals produced by the reaction between e^- and dissolved oxygen (DO). In the Cr(VI) and MO matrix, e^- is preferred to be consumed by DO to form **.**O_2^- radicals for MO degradation, which leads to the decrease of the Cr(VI) reduction efficiency. As displayed in Fig. 9(c), in the mixed MO/MB system, the degradation efficiencies are similar to the mono-component degradation efficiencies.

The Mott-Schottky determination has been conducted to reveal the flat-band potentials of the **BUC-85** and **BUC-86** samples in this study (Fig. 10a and b) and the results indicated that they are typical *n*-type semiconductors due to the positive slopes. The E_{CB} values deduced from the Mott Schottky plots are about −0.349 and

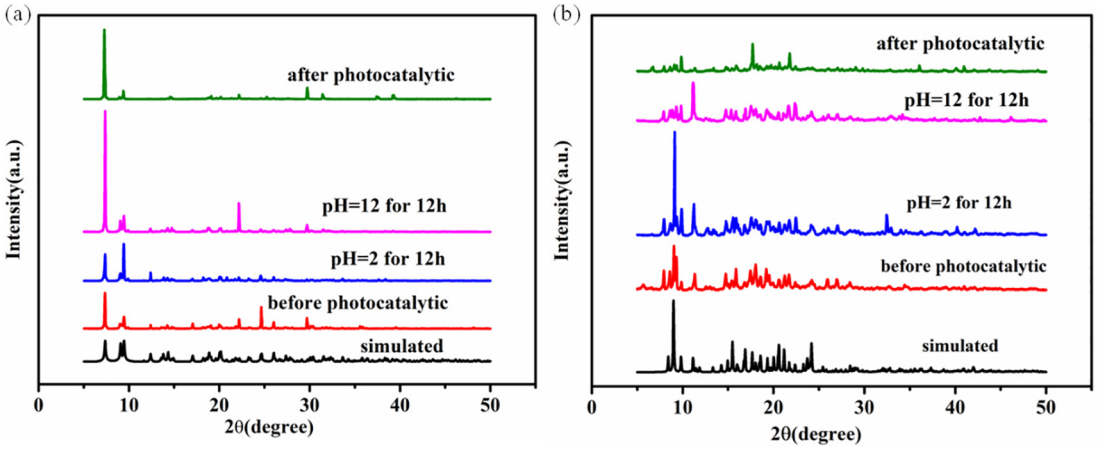

Fig. 8. PXRD patterns of before and after the photocatalytic reaction, immersed in H_2SO_4 or NaOH for 12 h and the simulated XRD pattern from the single-crystal structure data of **BUC-85** (a) and **BUC-86** (b).

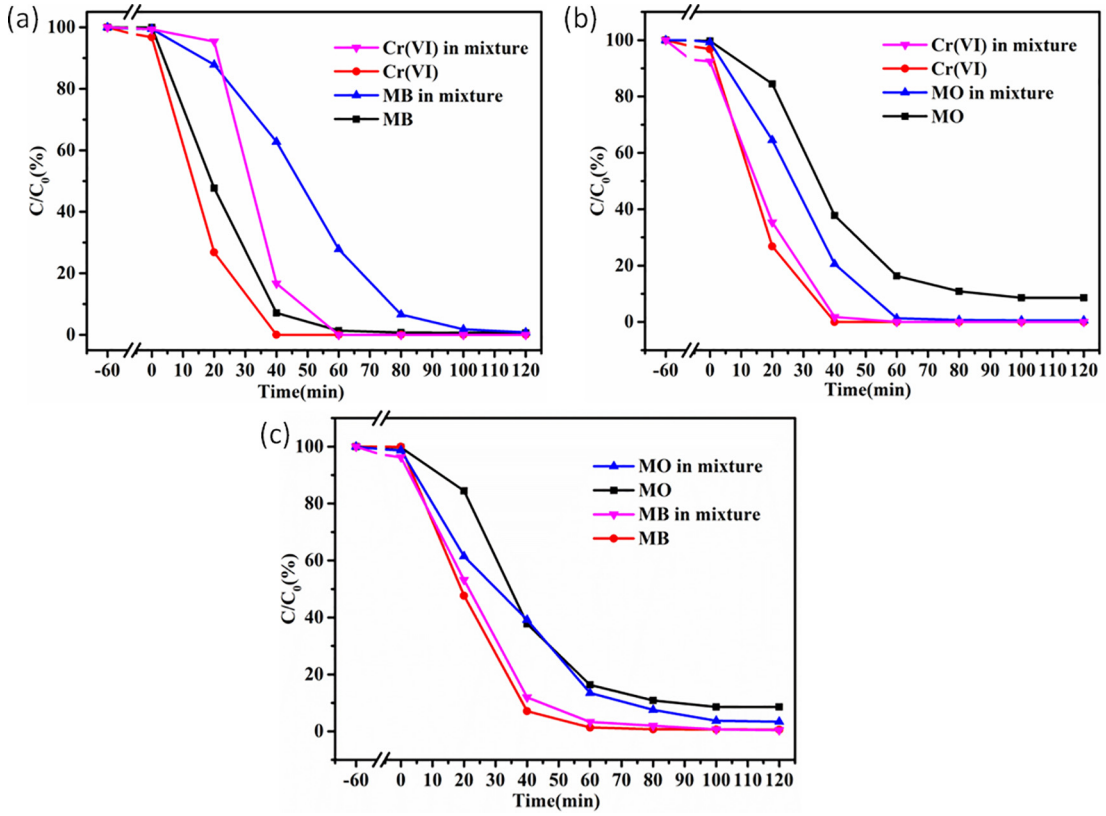

Fig. 9. The photocatalytic efficiencies of Cr(VI) removal and MO oxidation in their mono-component systems and in their intermixtures with **BUC-86 (a)** as a photocatalyst; The photocatalytic efficiencies of Cr(VI) removal and MB oxidation in their mono-component systems and in their intermixture with **BUC-86 (b)** as a photocatalyst; The photocatalytic efficiencies of MB and MO oxidation in their mono-component systems and in their intermixture with **BUC-86 (c)** as a photocatalyst. Conditions: 200 mL of Cr (VI) = 10 mg/L or MO = 10 mg/L or MB = 10 mg/L, photocatalyst dosage = 20 mg, pH = 2.0.

−0.333 eV (*vs.* Ag/AgCl, pH = 2.0) for **BUC-85** and **BUC-86**, respectively. Based on the bandgap values of **BUC-85** and **BUC-86**, the calculated valence band potentials (E_{VB}) are 3.297 and 3.789 eV, respectively [52–54].

Additionally, the rates of charge migration and recombination in the as-prepared photocatalysts were studied by photocurrent analysis and electrochemical impedance spectroscopy (EIS). A smaller Nyquist radius implies a smaller corresponding charge transfer resistance. Faster electron travel might result from a smaller Nyquist radius. As shown in Fig. 10c, the arc radius of **BUC-85** is less than that of **BUC-86**, indicating that the photo-induced holes and electrons over **BUC-85** are efficiently separated to accomplish the higher photocatalytic activity [33,47,53].

Except for MOF-5, most CPs belong to the class of molecular photocatalysts, whose mechanisms are usually explained in terms of frontier molecular orbital theory [55]. Possible mechanisms for the photocatalytic reduction of Cr(VI) ions and the degradation of organic dyes of these CPs are proposed. In Fig. 10d, upon UV light irradiation, **BUC-85** and **BUC-86** absorb photons and excite electrons (e^-) from the highest occupied molecular orbital (HOMO)

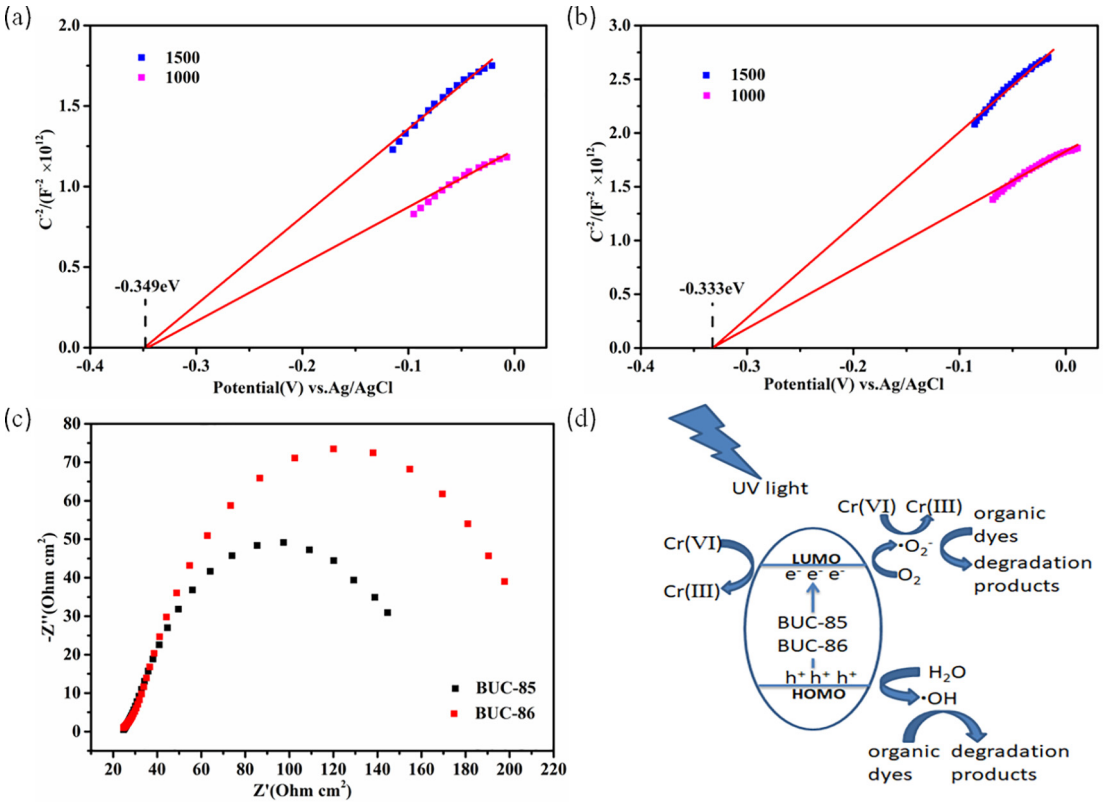

Fig. 10. The Mott-Schottky curves of **BUC-85 (a)** and **BUC-86 (b)**; (c) The EIS of **BUC-85** and **BUC-86**; (d) The proposed photocatalytic reaction mechanism of Cr(VI) removal and organic dyes oxidation with **BUC-85** and **BUC-86**.

and leave holes (h^+) in the lowest unoccupied molecular orbital (LUMO) [56]. The photo-induced electronic holes (h^+) in the LUMO either take part in the reduction of Cr(VI) to Cr(III) ions directly, or are transferred to generate **.**O_2^-, which achieves Cr(VI) reduction and organic pollutant oxidation. Additionally, the HOMO strongly demands electrons to return to its stable state, therefore one electron is captured from water molecules and the product **.**OH active species. The **.**OH radicals can further destroy organic dyes efficiently. In general, **BUC-85** and **BUC-86** provide a good platform to promote the transfer of photoelectrons and inhibit the combination of photo-generated electron-holes [32,57].

4. Conclusions

In short, two new CPs, **BUC-85** and **BUC-86**, have been prepared under hydrothermal conditions. Both CPs are highly efficient heterogeneous photocatalysts which can be used for Cr(VI) reduction and dye degradation under the irradiation of UV light. The active species capture experiments results affirmed that **.**OH is the major active species in the dye degradation reactions. More significantly, these two bifunctional CPs can simultaneously accomplish Cr(VI) reduction and oxidative organic pollutant degradation, which makes the two CPs potential photocatalyst candidates for environmental restoration.

CRediT authorship contribution statement

Si-Qi Ma: Methodology, Validation, Formal analysis, Investigation, Writing - original draft, Data curation, Visualization. **Baoyi Yu:** Software, Resources, Supervision, Project administration, Funding acquisition. **Xiao-Hong Yi:** Validation, Formal analysis, Investigation, Data curation, Visualization. **Chong-Chen Wang:** Conceptualization, Software, Resources, Writing - review & editing, Supervision, Project administration, Funding acquisition.

Declaration of Competing Interest

The authors declare that they have no known competing financial interests or personal relationships that could have appeared to influence the work reported in this paper.

Acknowledgements

This work was supported by the National Natural Science Foundation of China (51878023), Beijing Natural Science Foundation (No. 8202016), Great Wall Scholars Training Program Project of Beijing Municipality Universities (CIT&TCD20180323), Project of Construction of Innovation Teams and Teacher Career Development for Universities and Colleges Under Beijing Municipality (IDHT20170508), and the Beijing Talent Project (2019A22).

Appendix A. Supplementary data

Supplementary data to this article can be found online at https://doi.org/10.1016/j.poly.2020.114701.

References

[1] Y.-X. Li, H. Fu, P. Wang, C. Zhao, W. Liu, C.-C. Wang, Porous tube-like ZnS derived from rod-like ZIF-L for photocatalytic Cr(VI) reduction and organic pollutants degradation, Environ. Pollut. 256 (2020) 113417.
[2] K. Zhu, C. Chen, S. Lu, X. Zhang, A. Alsaedi, T. Hayat, MOFs-induced encapsulation of ultrafine Ni nanoparticles into 3D N-doped graphene-CNT frameworks as a recyclable catalyst for Cr(VI) reduction with formic acid, Carbon 148 (2019) 52–63.

[3] J. Qiu, X.-F. Zhang, X. Zhang, Y. Feng, Y. Li, L. Yang, H. Lu, J. Yao, Constructing $Cd_{0.5}Zn_{0.5}S$@ZIF-8 nanocomposites through self-assembly strategy to enhance Cr(VI) photocatalytic reduction, J. Hazard. Mater. 349 (2018) 234–241.

[4] R. Liang, L. Shen, F. Jing, W. Wu, N. Qin, R. Lin, L. Wu, NH_2-mediated indium metal–organic framework as a novel visible-light-driven photocatalyst for reduction of the aqueous Cr(VI), Appl. Catal. B: Environ. 162 (2015) 245–251.

[5] J. Zhong, X.-H. Yi, P. Wang, C.-C. Wang, A stable 1D mixed-valence CuI/CuII coordination polymer with photocatalytic reduction activity toward Cr(VI), J. Mol. Struct. 1183 (2019) 256–262.

[6] X. Wang, W. Liu, H. Fu, X.-H. Yi, P. Wang, C. Zhao, C.-C. Wang, W. Zheng, Simultaneous Cr(VI) reduction and Cr(III) removal of bifunctional MOF/Titanate nanotube composites, Environ. Pollut. 249 (2019) 502–511.

[7] L. Shi, T. Wang, H. Zhang, K. Chang, X. Meng, H. Liu, J. Ye, An Amine-functionalized iron(III) metal-organic framework as efficient visible-light photocatalyst for Cr(VI) reduction, Adv. Sci. 2 (2015) 1500006.

[8] Y.-C. Zhou, P. Wang, H. Fu, C. Zhao, C.-C. Wang, Ternary Ag/Ag_3PO_4/MIL-125-NH_2 Z-scheme heterojunction for boosted photocatalytic Cr(VI) cleanup under visible light, Chin. Chem. Lett. (2020), https://doi.org/10.1016/j.cclet.2020.02.048.

[9] X.-H. Yi, S.-Q. Ma, X.-D. Du, C. Zhao, H. Fu, P. Wang, C.-C. Wang, The facile fabrication of 2D/3D Z-scheme g-C_3N_4/UiO-66 heterojunction with enhanced photocatalytic Cr(VI) reduction performance under white light, Chem. Eng. J. 375 (2019) 121944.

[10] H.-C. Li, W.-J. Liu, H.-X. Han, H.-Q. Yu, Hydrophilic swellable metal–organic framework encapsulated Pd nanoparticles as an efficient catalyst for Cr(vi) reduction, J. Mater. Chem. A. 4 (2016) 11680–11687.

[11] J.J. Testa, M.A. Grela, M.I. Litter, Heterogeneous photocatalytic reduction of chromium(VI) over TiO_2 particles in the presence of oxalate: Involvement of Cr (V) species, Environ. Sci. Technol. 38 (2004) 1589–1594.

[12] D.-M. Chen, C.-X. Sun, C.-S. Liu, M. Du, Stable layered semiconductive Cu(I)–organic framework for efficient visible-light-driven Cr(VI) reduction and H_2 evolution, Inorg. Chem. 57 (2018) 7975–7981.

[13] H. Ramezanalizadeh, F. Manteghi, Synthesis of a novel MOF/$CuWO_4$ heterostructure for efficient photocatalytic degradation and removal of water pollutants, J. Clean. Prod. 172 (2018) 2655–2666.

[14] S. Mosleh, M.R. Rahimi, M. Ghaedi, K. Dashtian, S. Hajati, $BiPO_4$/Bi_2S_3-HKUST-1-MOF as a novel blue light-driven photocatalyst for simultaneous degradation of toluidine blue and auramine-O dyes in a new rotating packed bed reactor: optimization and comparison to a conventional reactor, RSC Adv. 6 (2016) 63667–63680.

[15] X.-D. Du, X.-H. Yi, P. Wang, W. Zheng, J. Deng, C.-C. Wang, Robust photocatalytic reduction of Cr(VI) on UiO-66-NH_2(Zr/Hf) metal-organic framework membrane under sunlight irradiation, Chem. Eng. J. 356 (2019) 393–399.

[16] P. Li, M. Guo, Q. Wang, Z. Li, C. Wang, N. Chen, C.-C. Wang, C. Wan, S. Chen, Controllable synthesis of cerium zirconium oxide nanocomposites and their application for photocatalytic degradation of sulfonamides, Appl. Catal. B: Environ. 259 (2019) 118107.

[17] D.-D. Chen, X.-H. Yi, C. Zhao, H. Fu, P. Wang, C.-C. Wang, Polyaniline modified MIL-100(Fe) for enhanced photocatalytic Cr(VI) reduction and tetracycline degradation under white light, Chemosphere 245 (2019) 125659.

[18] S.B. Bagherzadeh, M. Kazemeini, N.M. Mahmoodi, A study of the DR23 dye photocatalytic degradation utilizing a magnetic hybrid nanocomposite of MIL-53(Fe)/CoF_e2_O4: Facile synthesis and kinetic investigations, J. Mol. Liq. 301 (2020) 112427.

[19] S. Mosleh, M.R. Rahimi, M. Ghaedi, K. Dashtian, S. Hajati, Photocatalytic degradation of binary mixture of toxic dyes by HKUST-1 MOF and HKUST-1-SBA-15 in a rotating packed bed reactor under blue LED illumination: Central composite design optimization, RSC Adv. 6 (2016) 17204–17214.

[20] C.-Y. Wang, B. Yu, H. Fu, P. Wang, C.-C. Wang, A mixed valence Tb(III)/Tb(IV) metal–organic framework: Crystal structure, luminescence property and selective detection of naproxen, Polyhedron 159 (2019) 298–307.

[21] E.-H. Zhou, B.-H. Li, W.-X. Chen, Z. Luo, J. Liu, A. Singh, A. Kumar, J.-C. Jin, Photocatalytic degradation of organic dyes by a stable and biocompatible Zn (II) MOF having ferulic acid: Experimental findings and theoretical correlation, J. Mol. Struct. 1149 (2017) 352–356.

[22] G. Lin, H. Wang, X. Lai, R. Yang, Y. Zou, J. Wan, D. Liu, H. Jiang, Y. Hu, Co_3O_4 /N-doped RGO nanocomposites derived from MOFs and their highly enhanced gas sensing performance, Sens. Actuators B 303 (2020) 127219.

[23] J. Guo, J.-J. Li, C.-C. Wang, Adsorptive removal of Cr(VI) from simulated wastewater in MOF BUC-17 ultrafine powder, J. Environ. Chem. Eng. 7 (2019) 102909.

[24] X.-X. Song, H. Fu, P. Wang, H.-Y. Li, Y.-Q. Zhang, C.-C. Wang, The selectively fluorescent sensing detection and adsorptive removal of Pb^{2+} with a stable [δ-Mo_8O_{26}]-based hybrid, J. Colloid Interface Sci. 532 (2018) 598–604.

[25] A. Liu, C.-Z. Wang, C. Chu, H.-Y. Chu, X. Chen, A.-F. Du, J. Mao, W. Zheng, C.-C. Wang, Adsorption performance toward organic pollutants, odour control and anti-microbial activities of one Ag-based coordination polymer, J. Environ. Chem. Eng. 6 (2018) 4961–4969.

[26] W. Chen, B. Han, C. Tian, X. Liu, S. Liang, H. Deng, Z. Lin, MOFs-derived ultrathin holey Co_3O_4 nanosheets for enhanced visible light CO_2 reduction, Appl. Catal. B: Environ. 244 (2018) 996–1003.

[27] Y. Chen, D. Wang, X. Deng, Z. Li, Metal–organic frameworks (MOFs) for photocatalytic CO_2 reduction, Catal. Sci. Technol. 7 (2017) 4893–4904.

[28] S. Li, J. Tan, Z. Jiang, J. Wang, Z. Li, MOF-derived bimetallic Fe-Ni-P nanotubes with tunable compositions for dye-sensitized photocatalytic H_2 and O_2 production, Chem. Eng. J. 384 (2020) 123354.

[29] H. Fu, X.-X. Song, L. Wu, C. Zhao, P. Wang, C.-C. Wang, Room-temperature preparation of MIL-88A as a heterogeneous photo-Fenton catalyst for degradation of rhodamine B and bisphenol a under visible light, Mater. Res. Bull. 125 (2020) 110806.

[30] D. Pang, P. Wang, H. Fu, C. Zhao, C.-C. Wang, Highly efficient removal of As(V) using metal–organic framework BUC-17, SN Appl. Sci. 2 (2020) 184.

[31] F.-X. Wang, X. Chen, P. Wang, C.-C. Wang, New Zn/Cd coordination polymers constructed from mixed ligands: Crystal structures and photocatalytic performances toward organic dyes degradation, J. Inorg. Organomet. Polym. Mater. 28 (2018) 1565–1573.

[32] F.-X. Wang, X.-H. Yi, C.-C. Wang, J.-G. Deng, Photocatalytic Cr(VI) reduction and organic-pollutant degradation in a stable 2D coordination polymer, Chin. J. Catal. 38 (2017) 2141–2149.

[33] X.-H. Yi, F.-X. Wang, X.-D. Du, P. Wang, C.-C. Wang, Facile fabrication of BUC-21/g-C_3N_4 composites and their enhanced photocatalytic Cr(VI) reduction performances under simulated sunlight, Appl. Organomet. Chemi. 33 (2019) e4621.

[34] B.M. Rajbongshi, A. Ramchiary, S.K. Samdarshi, Influence of N-doping on photocatalytic activity of ZnO nanoparticles under visible light irradiation, Mater. Lett. 134 (2014) 111–114.

[35] H. Ramesh, K. Parthipan, P. Sambasiva Rao, EPR, FTIR, Powder XRD and Optical Absorption Studies of Cu(II) Ion in Triaqua(1,10-Phenanthroline-k2N,N′)(Sulfato-kO)Zinc(II), Appl. Magn. Reson., 40 (2011) 513-524.

[36] C.C. Wagner, E.J. Baran, Vibrational spectra of Zn(II) complexes of the amino acids with hydrophobic residues, Spectrochim. Acta A. 72 (2009) 936–940.

[37] X.-H. Yi, F.-X. Wang, X.-D. Du, H. Fu, C.-C. Wang, Highly efficient photocatalytic Cr(VI) reduction and organic pollutants degradation of two new bifunctional 2D Cd/Co-based MOFs, Polyhedron 152 (2018) 216–224.

[38] H. Wang, W. Yang, Z.-M. Sun, Mixed-Ligand Zn-MOFs for Highly Luminescent Sensing of Nitro Compounds, Chem. -Asian J. 8 (2013) 982–989.

[39] Y.-X. Shi, F.-L. Hu, W.-H. Zhang, J.-P. Lang, A unique Zn(ii)-based MOF fluorescent probe for the dual detection of nitroaromatics and ketones in water, CrystEngComm 17 (2015) 9404–9412.

[40] Y.L. Pan, J.F. Chen, J. Wang, Y. Zhang, D.X. Jia, Solvothermal synthesis and optical property of novel lanthanide(III) coordination polymers involving inorganic tridentate μ-η1, η2-Sb_S4 S-donor ligand, Inorg. Chem. Commun. 13 (2010) 1569–1571.

[41] J.-L. Du, X.-Y. Zhang, C.-P. Li, J.-P. Gao, J.-X. Hou, X. Jing, Y.-J. Mu, L.-J. Li, A bi-functional luminescent Zn(II)-MOF for detection of nitroaromatic explosives and Fe^{3+} ions, Sensor. Actuat. B-Chem. 257 (2018) 207–213.

[42] A. Crake, K.C. Christoforidis, A. Kafizas, S. Zafeiratos, C. Petit, CO_2 capture and photocatalytic reduction using bifunctional TiO_2/MOF nanocomposites under UV–vis irradiation, Appl. Catal. B: Environ. 210 (2017) 131–140.

[43] J. Li, W. Gou, Y. Zhou, Z.-F. Lin, F. Peng, A Zn(II)/anthracene coordination polymer showing highly efficient photocatalytic Cr(VI) reduction in aqueous solution, Inorg. Chem. Commun. 101 (2019) 52–56.

[44] Q. Gao, D. Lin, Y. Fan, Q. He, Q. Wang, Visible light induced photocatalytic reduction of Cr(VI) by self-assembled and amorphous Fe-2MI, Chem. Eng. J. 374 (2019) 10–19.

[45] H. Wang, X. Yuan, Y. Wu, G. Zeng, X. Chen, L. Leng, Z. Wu, L. Jiang, H. Li, Facile synthesis of amino-functionalized titanium metal-organic frameworks and their superior visible-light photocatalytic activity for Cr(VI) reduction, J. Hazard. Mater. 286 (2015) 187–194.

[46] R. Yuan, C. Yue, J. Qiu, F. Liu, A. Li, Highly efficient sunlight-driven reduction of Cr(VI) by TiO_2@NH_2-MIL-88B(Fe) heterostructures under neutral conditions, Appl. Catal. B: Environ. 251 (2019) 229–239.

[47] Y.-C. Zhou, X.-Y. Xu, P. Wang, H. Fu, C. Zhao, C.-C. Wang, Facile fabrication and enhanced photocatalytic performance of visible light responsive UiO-66-NH_2/Ag_2CO_3 composite, Chin. J. Catal. 40 (2019) 1912–1923.

[48] C. Zhao, Z. Wang, X. Li, X. Yi, H. Chu, X. Chen, C.-C. Wang, Facile fabrication of BUC-21/$Bi_{24}O_{31}Br_{1}0$ composites for enhanced photocatalytic Cr(VI) reduction under white light, Chem. Eng. J. 389 (2020) 123431.

[49] M. Jahurul Islam, H.K. Kim, D. Amaranatha Reddy, Y. Kim, R. Ma, H. Baek, J. Kim, T.K. Kim, Hierarchical BiOI nanostructures supported on a metal organic framework as efficient photocatalysts for degradation of organic pollutants in water, Dalton Trans. 46 (2017) 6013–6023.

[50] C.-F. Zhang, L.-G. Qiu, F. Ke, Y.-J. Zhu, Y.-P. Yuan, G.-S. Xu, X. Jiang, A novel magnetic recyclable photocatalyst based on a core–shell metal–organic framework Fe_3O_4@MIL-100(Fe) for the decolorization of methylene blue dye, J. Mater. Chem. A 1 (2013) 14329–14334.

[51] Y.-X. Li, X. Wang, C.-C. Wang, H. Fu, Y. Liu, P. Wang, C. Zhao, S-TiO_2/UiO-66-NH_2 composite for boosted photocatalytic Cr(VI) reduction and bisphenol A degradation under LED visible light, J. Hazard. Mater. 399 (2020) 123085.

[52] R. Liang, Z. Liang, F. Chen, D. Xie, Y. Wu, X. Wang, G. Yan, L. Wu, Sodium dodecyl sulfate-decorated MOF-derived porous Fe_2O_3 nanoparticles: High performance, recyclable photocatalysts for fuel denitrification, Chin. J. Catal. 41 (2020) 188–199.

[53] C. Yang, X. You, J. Cheng, H. Zheng, Y. Chen, A novel visible-light-driven In-based MOF/graphene oxide composite photocatalyst with enhanced photocatalytic activity toward the degradation of amoxicillin, Appl. Catal. B: Environ. 200 (2017) 673–680.

[54] R. Lin, S. Li, J. Wang, J. Xu, C. Xu, J. Wang, C. Li, Z. Li, Facile generation of carbon quantum dots in MIL-53(Fe) particles as localized electron acceptors for enhancing their photocatalytic Cr(vi) reduction, Inorg. Chem. Front. 5 (2018) 3170–3177.
[55] M. Alvaro, E. Carbonell, B. Ferrer, F.X. LlabrésiXamena, H. Garcia, Semiconductor Behavior of a Metal-Organic Framework (MOF), Chem. Eur. J., 13 (2007) 5106-5112.
[56] C. Gao, J. Wang, H. Xu, Y. Xiong, Coordination chemistry in the design of heterogeneous photocatalysts, Chem. Soc. Rev. 46 (2017) 2799–2823.
[57] M.-J. Wei, J.-H. Zhang, W.-M. Liao, Z.-W. Wei, M. Pan, C.-Y. Su, A novel Co-O cluster based coordination polymer for efficient hydrogen production photocatalysis, J. Photochem. Photobiol. A 387 (2020) 112137.